2017

A New Approach to Model Reduction of Nonlinear Control Systems Using Smooth Orthogonal Decomposition

Shahab Ilbeigi
University of Rhode Island

David Chelidze
University of Rhode Island, chelidze@uri.edu

Citation/Publisher Attribution

Ilbeigi S, Chelidze D. A new approach to model reduction of nonlinear control systems using smooth orthogonal decomposition. *Int J Robust Nonlinear Control*. 2018;28:4367–4381. https://doi.org/10.1002/rnc.4238
Available at: https://doi.org/10.1002/rnc.4238

A New Approach to Model Reduction of Nonlinear Control Systems Using Smooth Orthogonal Decomposition

Shahab Ilbeigi **David Chelidze***
Department of Mechanical, Industrial and Systems Engineering
University of Rhode Island, Kingston, RI 02881

Draft Copy, May 25, 2017

Abstract

A new approach to model order reduction of nonlinear control systems is aimed at developing persistent reduced order models *(ROMs) that are robust to the changes in system's energy level. A multivariate analysis method called* smooth orthogonal decomposition *(SOD) is used to identify the dynamically relevant modal structures of the control system. The identified SOD subspaces are used to develop persistent ROMs. Performance of the resultant SOD-based ROM is compared with* proper orthogonal decomposition *(POD)-based ROM by evaluating their robustness to the changes in system's energy level. Results show that SOD-based ROMs are valid for a relatively wider range of the nonlinear control system's energy when compared with POD-based models. In additions, the SOD-based ROMs show considerably faster computation times compared to the POD-based ROMs of same order. For the considered dynamic system SOD provides more effective reduction in dimension and complexity compared to POD.*

Keywords: *nonlinear model reduction, proper orthogonal decomposition, smooth orthogonal decomposition, nonlinear control systems, subspace robustness.*

1 Introduction

A high-fidelity mathematical model is essential to control a complex nonlinear dynamical system. These models are often high-dimensional, which means that complex differential equations are needed to describe them. Therefore, in many cases, they may not be computationally tractable. This makes the real-time control difficult to implement. A *reduced order model* (ROM) of a complex system can result in a computationally tractable accurate model for the control system [1].

Computationally complex dynamical systems usually evolve on a lower-dimensional curved nonlinear manifold embedded in a higher dimensional state space of the system. Geometric structures of nonlinear manifolds have not been extensively incorporated in nonlinear control theory since identification of high-dimensional manifold is difficult [2–4]. Also, even if we overcome this problem, the stability and accuracy of the reduced model is still guaranteed only for a small range of operating conditions or modal parameters [4].

In this paper, we use *smooth orthogonal decomposition* (SOD) [5–7] as a new tool for model order reduction (MOR) for nonlinear control systems. Our method is categorized under Galerkin projection based reduced order modeling which projects the high-dimensional nonlinear system onto an appropriate linear subspace to yield a lower-dimensional system. We also use a new metric to evaluate the persistency of the identified linear subspaces. A persistent linear subspace is robust to the changes in system's operating conditions and thus expands a region within the

*email: chelidze@uri.edu ⋄ phone: 401.874.2356 ⋄ fax: 401.874.2355 ⋄ web: mcise.uri.edu/chelidze/

system's state space in which the ROM is valid. We aim to obtain a persistent ROM which allows the control system to globally operate within a region of interest.

Projection onto the linear subspace does not negate the nonlinearity of the original system [8]. While the resultant ROM for the control system is still nonlinear, its corresponding state is low-dimensional which makes the control system computationally manageable. Reduced order modeling of dynamical systems targets the computational time of the model simulations.

For nonlinear control systems, however, we examine the output of the persistent ROM for a given input in comparison to the output of the full-scale control model. For the input we use a set of impulse functions as random input. This approach has two advantages: (1) under random input it would be difficult to stay in a limited region of the space; and (2) random input imitates the non-deterministic impulses generated by the control scheme as inputs to the system.

For the purpose of this work we consider the model presented in [1]. We describe and apply SOD as a new reduced order modeling method for nonlinear control systems. We also formalize the subspace robustness as a metric to identify the persistent subspaces for reduced order control models in such a way that they are globally valid for a range of the system's energy. Finally, the developed methodology of this paper will be tested using numerical simulations of a nonlinear control system.

1.1 Background and Prior Work

Within the realm of complex dynamical systems, reduced order modeling is being extensively used to reduce the redundant computations and data storage requirement [7, 9–14]. We place the majority of reduced order modeling methods for dynamical system into two main categories. In the first category, ROMs are obtained by projecting a system onto a lower-dimensional subspace. In the second, the identified nonlinear manifolds or *nonlinear normal modes* are used to obtain ROMs.

The methodologies for obtaining low-dimensional subspaces in the first category of MOR are, though not limited to, *linear normal modes* [15, 16], *proper orthogonal decomposition* (POD) (also known as singular value decomposition, principal component analysis, or Karhunen-Loève expansion) [8, 17–23], and SOD [5–7, 24]. In addition, Krylov subspace projections [25], Hankel norm approximations [26–29], and truncated balance realizations [30, 31] are to be mentioned. For the second category, the nonlinear coordinate transformation can be either approximated analytically, by the techniques such as multiple scales [32–36] and harmonic balance [37], or numerically, by the methods discussed in [36].

The research on MOR of control systems is extensive. It includes well understood, and established theories and methodologies for reduction of linear control systems. Examples of these methods are POD, used for instance to design control systems for PDEs [38, 39] and optimal control of fluids [40], Hankel norm approximation [26, 41, 42], and balanced truncation [43] which was proposed by Moore [44]. The reader may review other methods for MOR for linear control system in Refs. [43, 45, 46].

Model reduction of nonlinear control systems is not as well understood as for linear systems. For example, POD is being frequently used [47], however, it suffers from some limitations that are discussed in [48]: POD-based models are very sensitive to the data used [8] and may become unstable even near stable equilibrium points [49]. Another method is balanced truncation which is developed for nonlinear control system in two distinct approaches: one is based on energy function used in the works by Scherpen [50–53] and the other is proposed by Lall based on empirical balanced truncation [1].

2 Model Reduction Using Galerkin Projection

We consider a nonlinear control system in the form:

$$\begin{aligned} \dot{\mathbf{y}}(t) &= \mathbf{f}(\mathbf{y}(t)\,, \mathbf{u}(t)) \\ \mathbf{z}(t) &= \mathbf{h}(\mathbf{y}(t))\,, \end{aligned} \tag{1}$$

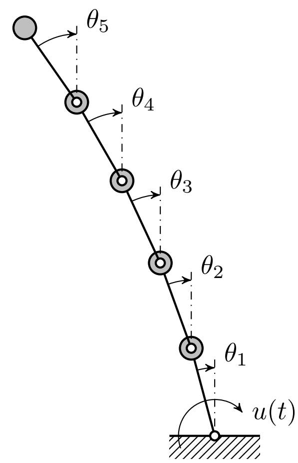

Figure 1: Schematic of the nonlinear control system

where $\mathbf{y} \in \mathbb{R}^{2n}$ is state vector of the system, n is number of degrees-of-freedom, t is time, $\mathbf{f} : \mathbb{R}^{2n} \times \mathbb{R}^{p} \to \mathbb{R}^{2n}$ is a nonlinear flow function describing the dynamics of the system, $\mathbf{u}(t) \in \mathbb{R}^{p}$ is the input to the system, and $\mathbf{z}(t) \in \mathbb{R}^{w}$ is the system output or the state vector which is based on the desired observation, $\mathbf{h} : \mathbb{R}^{2n} \to \mathbb{R}^{w}$. The goal of the control system is to control the output $\mathbf{z}(t)$, however, if the system is large-scale or highly nonlinear, we will aim to obtain a reduced order nonlinear control model. A reduced order control model is easier to implement and is essential for a real-time and accurate control.

Galerkin projection based MOR methods are based on transforming the $2n$-dimensional state vector $\mathbf{y}$ to a k-dimensional state vector $\mathbf{q}$, given that $k < 2n$. The transformation is performed by a full-rank projection matrix $\mathbf{P}_k \in \mathbb{R}^{2n \times k}$ in the form $\mathbf{q} = \mathbf{P}_k^{\dagger}\mathbf{y}$, with $(.)^{\dagger}$ defined as the pseudoinverse of $(.)$, to yield the reduced order model:

$$\begin{aligned} \dot{\mathbf{q}}(t) &= \mathbf{P}_k^{\dagger}\mathbf{f}(\mathbf{P}_k\mathbf{q}(t), \mathbf{u}(t))\,, \\ \mathbf{z}(t) &= \mathbf{h}(\mathbf{P}_k\mathbf{q}(t))\,. \end{aligned} \tag{2}$$

Matrix $\mathbf{P}$ represents a description of the modal space of a dynamical system. Matrix $\mathbf{P}_k$ is the k-dimensional modal sub-space formed by k dominant modes of the modal space. While it can be analytically obtained for linear dynamical systems using linear normal modes theory, another method to obtain $\mathbf{P}$, regardless of system's linearity or nonlinearity, is using multivariate analysis of its response. Multivariate analysis is applied to the data matrices from the full model simulations or experiments. In this work, all the data matrices are obtained from simulations. We first describe a new multivariate analysis method with advantages over the conventional methods like POD. Before proceeding to the theory and methodology of this paper, we present an example of a nonlinear control system derived from the work by Lall *et al.* [1] in which they developed the *balanced truncation* method for nonlinear control systems.

2.1 Mathematical Model of Nonlinear Control System

In this section, we model the system adopted from [1]. The system, shown in Fig. 1, consists of 5 weightless links with the length of $2l$ which are connected to each other by torsional springs and dampers. Springs and dampers are not drawn for the sake of clarity. The first link is pinned to the ground and driven by a torque as the input to the system. The coordinate θ_i measures the angular position of the i-th link as shown in the figure. We obtain the governing differential equation of the system using the Lagrange's equation:

$$\frac{d}{dt}\left(\frac{\partial T}{\partial \dot{\theta}_i}\right) - \frac{\partial T}{\partial \theta_i} + \frac{\partial V}{\partial \theta_i} = F_i, \quad (\text{for } i = 1, \ldots, n) \tag{3}$$

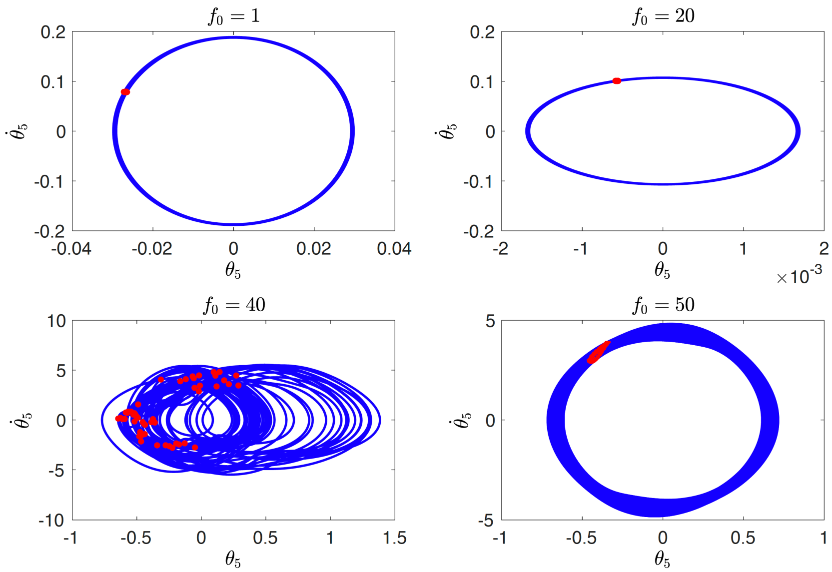

Figure 2: This figure shows the different values for which the different phase space figure have been obtained.

where V and T are potential and kinetic energy, and F_i is the generalized forcing term. Now we consider $\mathbf{y} = [\theta_1, \ldots, \theta_5, \dot{\theta}_1, \ldots, \dot{\theta}_5]^T$ to be the state vector. By substituting the state vector in the equations of motion, we obtain its state space form:

$$\mathbf{M}\big(\mathbf{y}(t)\big)\, \dot{\mathbf{y}}(t) = \mathbf{L}\mathbf{y}(t) + \mathbf{f}_{\mathrm{n}}(\mathbf{y}(t)) + \mathbf{u}(t)\,, \tag{4}$$

in which $\mathbf{M}\big(\mathbf{y}(t)\big)$ is the time-varying mass matrix and $\mathbf{L}$ is the matrix of the linear terms. Both are given in Appendix A. Also, $\mathbf{f}_{\mathrm{n}}$ is the vector of the nonlinear terms and $\mathbf{u}(t)$ is the single input to the system. The output of the system is defined as the horizontal position of the tip of the 5th link

$$z = 2l \sum_{i=1}^{5} \sin y_i \tag{5}$$

and is to be controlled.

We simulate Eq. (4) as a full-scale model of the control system using harmonic excitation, $u(t) = f_0 \sin \omega t$. Fig. 2 depicts the phase portraits of the fifth link for different forcing amplitude values. It shows how the system is in the approximately linear regime for $f_0 = 1$ and transitions into the nonlinear regime for higher f_0 values. The periodicity of the results is shown by Poincare maps in the figures. The system has an indication of chaos for $f_0 = 40$, indication of quasiperiodicity for $f_0 = 50$, and is periodic for the other amplitudes. To obtain this figure, the system is excited with frequency of $1\,\mathrm{Hz}$, which is close to the third linear modal frequency. The oscillations are recorded for 500 sec which is equal to 500 cycles of harmonic forcing, however, only the last 50 cycles are shown in the phase portraits in order to get rid of the transient behavior in the visualizations.

2.2 Multivariate Analysis Method

As mentioned earlier, each data-based method identifies a modal structure of the system described by $\mathbf{P}$ for MOR. There are many different approaches to do so but here we use SOD, a relatively new multivariate analysis method. SOD can be viewed as an extension to POD and thus, similarly, we use the simulation results to form data matrices for multivariate analysis. The data provide us with the information on the state of the control system to a defined input $\mathbf{u}(t)$ over a specified period of time.

We record the state variable measurements of the full-scale system, described by Eq. (4) to form a position and velocity data matrices $\mathbf{X} \in \mathbb{R}^{r\times n}$ and $\mathbf{V} \in \mathbb{R}^{r\times n}$, respectively. $\mathbf{X}$ is composed of r snapshots of n position state variables. Similarly, $\mathbf{V}$ is composed of r snapshots of n velocity state variables. Thus, the data matrix $\mathbf{Y}$ is given as $\mathbf{Y} = [\mathbf{X}\ \mathbf{V}]$.

The time derivative of $\mathbf{X}$ is $\mathbf{V}$. To obtain a time derivative of $\mathbf{V}$ or an acceleration data matrix $\mathbf{A}$, we can use a full model of our dynamical system, Eq. (4). Alternatively, for experimental data, it can be approximated by $\mathbf{A} \approx \mathbf{DV}$, where $\mathbf{D}$ is the matrix form of some differential operator such as forward difference. Therefore, an ensemble of time derivative of $\mathbf{Y}$ will be $\dot{\mathbf{Y}} = [\mathbf{V}\ \mathbf{A}]$. Provided that $\mathbf{Y}$ and $\dot{\mathbf{Y}}$ are zero mean, the corresponding auto-covariance matrices can be formed by

$$\mathbf{\Sigma}_{yy} = \frac{1}{r-1}\mathbf{Y}^{\mathrm{T}}\mathbf{Y}\,, \quad \mathbf{\Sigma}_{\dot{y}\dot{y}} = \frac{1}{r-1}\dot{\mathbf{Y}}^{\mathrm{T}}\dot{\mathbf{Y}}\,. \tag{6}$$

Prior to explaining SOD, we will briefly discuss POD.

2.2.1 Proper Orthogonal Decomposition

In POD, we are looking for a basis vector $\phi \in \mathbb{R}^{2n}$ such that a projection of the data matrix onto this vector has maximal variance. The description of POD translates into the following constrained maximization problem:

$$\max_{\phi} \|\mathbf{Y}\phi\|^2 \text{ subject to } \|\phi\| = 1\,.$$

We obtain the solution to the POD problem by solving the eigenvalue problem of the auto-covariance matrix $\mathbf{\Sigma}_{yy}$:

$$\mathbf{\Sigma}_{yy}\phi_k = \lambda_k\phi_k\,, \tag{7}$$

where λ_k are proper orthogonal values (POVs), $\phi_k \in \mathbb{R}^{2n}$ are proper orthogonal modes (POMs), and proper orthogonal coordinates (POCs) are columns of $\mathbf{Q} = \mathbf{Y}\Phi$, in which $\Phi = [\phi_1, \phi_2, \ldots, \phi_{2n}] \in \mathbb{R}^{2n\times 2n}$. POVs are ordered such that $\lambda_1 \geq \lambda_2 \geq \ldots \geq \lambda_{2n}$, and reflect the variances in $\mathbf{Y}$ data along the corresponding POMs.

2.2.2 Smooth Orthogonal Decomposition

In SOD, we are looking for a basis vector $\psi \in \mathbb{R}^{2n}$ such that a projection of the data matrix onto this vector has both minimal roughness and maximal variance. This description of SOD can be translated to the following mathematical form:

$$\max_{\psi} \|\mathbf{Y}\psi\|^2 \text{ subject to } \min_{\psi} \|\dot{\mathbf{Y}}\psi\|^2\,,$$

or

$$\max_{\psi} \left\{ \lambda(\psi) = \frac{\|\mathbf{Y}\psi\|^2}{\|\dot{\mathbf{Y}}\psi\|^2} \right\}.$$

The solution to the SOD problem, is achieved by solving a generalized eigenvalue problem of the matrix pair $\mathbf{\Sigma}_{yy}$ and $\mathbf{\Sigma}_{\dot{y}\dot{y}}$ in Eq. (6):

$$\mathbf{\Sigma}_{yy}\psi_k = \lambda_k \mathbf{\Sigma}_{\dot{y}\dot{y}}\psi_k\,, \tag{8}$$

where λ_k are *smooth orthogonal values* (SOVs), $\psi_k \in \mathbb{R}^{2n}$ are *smooth projection modes* (SPMs), and *smooth orthogonal coordinates* (SOCs) are given by $\mathbf{Q} = \mathbf{Y}\Psi$, where $\Psi = [\psi_1, \psi_2, \ldots, \psi_{2n}] \in \mathbb{R}^{2n\times 2n}$. Also, *smooth orthogonal modes* (SOMs) are $\Phi = \Psi^{-T}$. The degree of smoothness of the coordinates is described by the magnitude of the corresponding SOV. Thus, the greater magnitude of the SOV, the smoother in time is the corresponding coordinate. It should be noted that if we were to replace $\mathbf{\Sigma}_{\dot{y}\dot{y}}$ with the identity matrix, the formulation will yield the POD.

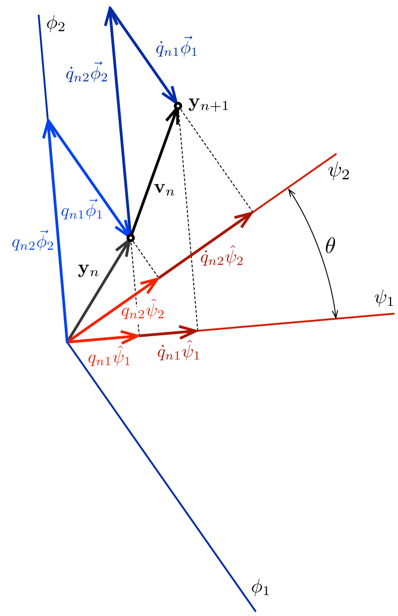

Figure 3: Geometrical interpretation of smooth orthogonal decomposition

2.2.3 Geometric Interpretation of SOD

Let as consider two consecutive samples $\mathbf{y}_n$ and $\mathbf{y}_{n+1}$ from a two-dimensional zero-mean field $\mathbf{Y} \in \mathbb{R}^{m\times 2}$ separated by the sampling time interval $\Delta t = 1$. Plot of these data points with the relevant axes is shown in Fig. 3. The first derivative of this field corresponding to $\mathbf{y}_n$ can be approximated as $\mathbf{v}_n \approx (\mathbf{y}_{n+1} - \mathbf{y}_n)/\Delta t = \mathbf{y}_{n+1} - \mathbf{y}_n$. We refer to this as *velocity vector* and depict it by a black vector between data points n and $n+1$.

We aim to obtain two SOMs, ϕ_1 and ϕ_2, and the corresponding bi-orthogonal pair of SPMs, ψ_1 and ψ_2, as a solution to SOD optimization (maximization) problem for the two-dimensional case. For simplicity, let $\hat{\psi}_i$ $(i = 1, 2)$ be unit vectors along the SPM directions. Then the corresponding SOM $\vec{\phi}_1$ will be perpendicular to $\hat{\psi}_2$ with magnitude equal to $(\cos\theta)^{-1}$, where θ is the angle between the SPMs. Similarly, $\vec{\phi}_2$ will be perpendicular to $\hat{\psi}_1$ and with the same magnitude $(\cos\theta)^{-1}$.

The projection of $\mathbf{y}_n$ onto ψ_1 and ψ_2 are shown as light red vectors and have magnitudes $q_{ni} = \mathbf{y}_n^T\hat{\psi}_i$. The projection of $\mathbf{v}_n$ onto ψ_1 and ψ_2 are shown as dark red vectors and have magnitudes $\dot{q}_{ni} = \mathbf{v}_n^T\hat{\psi}_i$. Taking $\hat{\psi}_1$, to be a free vector wandering in the 2D space of the data, by definition, we first aim to maximize the norm of the projection of each data point $\mathbf{y}_n$ in $\mathbf{Y}$ onto this vector $\hat{\psi}_1$, or $\max_{\psi_1}\langle q_{n1}^2\rangle$. At the same time, we also try to minimize the norm of the projection of the corresponding velocity $\mathbf{v}_n$ vector onto the same $\hat{\psi}_1$, or $\min_{\psi_1}\langle \dot{q}_{n1}^2\rangle$. Once ψ_1 is found, we repeat the same process for ψ_2 in the null space **[DC: the null space is perpendicular, but ψ_2 does not have to!!!]** of ψ_1, etc. This optimization problem has two solutions, $\hat{\psi}_1$ and $\hat{\psi}_2$. Unlike POD, the orthogonality condition is relaxed and SPMs/SOMs are not necessarily orthogonal[1] to each other: ϕ_2 axis is not an obviously orthogonal to ϕ_1. Thus, we expand each point in our field into SOMs:

$$\mathbf{y}_n = q_{n1}\vec{\phi}_1 + q_{n2}\vec{\phi}_2\,. \tag{9}$$

Associated with each SOM is a SOV, denoted by $\lambda_k = \langle q_{nk}^2\rangle / \langle \dot{q}_{nk}^2\rangle$, which is the ratio of variances in data and its time derivatives along ψ_k or ϕ_k. The greatest SOV belongs to the first SOM along which the ratio is maximum. Compare this to the first POM along which only the variance of data is maximum. The second greatest SOV comes with the second SOM along which the ratio is (locally) maximum, and so on. Therefore, each SOV represents the dominance of its corresponding mode in terms of overall spatial variation and temporal smoothness of the coordinate.

[1] SOCs are orthogonal to each other: $\mathbf{Q}^T\mathbf{Q} = \mathbf{I}$.

The data points in $\mathbf{Y}$ come from the consecutive mapping of a system's state onto another state using a vector valued function (flow) $\mathbf{f}$. POD only considers the spatial or geometric consequences of this mapping and neglects temporal structure of the states evolution. In contrast, SOD considers both the geometrical features of states and their time evolution in terms of overall spatial variation and temporal smoothness of the corresponding coordinate.

2.3 Robustness of Modal Subspaces

A nonlinear system can exhibit different behaviors based on its level of energy, which include both approximately linear behavior near the stable equilibrium points and nonlinear behavior far from those equilibrium points. Our system shows similar behavior as we discussed in section 2.1. Closer to the equilibria the system is described by LNMs, while as we get farther the system evolves on the NNM manifold, which may also change shape as system energy changes. Therefore, as energy increases not only the angle of the linear subspace that we get from multivariate analysis of the data changes, but we may also need a higher dimensional subspace to capture the NNM of the system. Different data set from the system simulations with different inputs or initial conditions have different energy level. Therefore, their extracted modal matrices and the corresponding lower-dimensional subspaces may be different.

The data set from the simulations of the systems subjected to random forcing can be used for multivariate analysis. In order to illustrate the changes in the modal structure, we excite our nonlinear system by the white noise with a chosen cut-off frequency. We expect that as we increase the forcing amplitude, the higher frequencies in the system's response come into account. As a result the modal structure of the system, indicated by the subspaces, need to be altered to account for higher frequencies.

We need a metric that measures the difference in the modal structure of two different data sets which have different energy level. One possibility is to measure the minimal angle between their corresponding subspaces using the following definition.

Definition: The minimal angle for two nonzero subspaces $\mathcal{P}^1,\ \mathcal{P}^2 \in \mathbb{R}^k$ is defined to be the number $0 \leq \theta \leq \frac{\pi}{2}$ that satisfies:

$$\cos\theta = \max\left\{\mathbf{v}^T\mathbf{u} : \mathbf{u} \in \mathcal{P}^1,\ \mathbf{v} \in \mathcal{P}^2,\ \text{and}\ \|\mathbf{u}\| = \|\mathbf{v}\| = 1\right\}.$$

For example, we generate data sets with different energy levels by changing the initial condition of the unforced links system. The initial angular position and velocity of all links except the first one are set to zero. The initial conditions for the first link is selected from the range $-5 \leq \theta_1(0) \leq 5$ and $-2 \leq \dot{\theta}_1(0) \leq 2$. The data set for each individual selection of $\dot{\theta}_1(0)$ is simulated and recorded. POD and SOD are applied to each data set to extract the corresponding modal matrices $\mathbf{P}$. Using the minimal angle between two subspaces, we can estimate the changes in the k-dimensional subspaces of the estimated modal matrices for different data sets.

Figure 4 shows the angle between the 2D subspaces within the selected range for the initial conditions of the first link. We calculate the angles with respect to a reference 2D subspace, which is the subspace obtained from the point $(-1.5, -0.2)$ in the map. The color of the map indicates the angle of data set generated for its corresponding initial condition. For POD, the blue region is limited to two small regions in which the subspace is not changing. A sudden change in the subspace angle occurs when we increase the energy level and enter the red region. However, for SOD the blue region is bigger and the changes in the subspace angle is less abrupt when we pass the borders of the region. When we increase the subspace dimension, as depicted in Fig. 5, the size of the blue region for POD does not change. The color of the red region for POD changes to cyan. The blue and cyan regions still have a distinct border indicating a sudden change in the subspaces with the increase in energy level. For SOD, in contrast, we observe that the increase in the subspace dimension spreads the blue region through the space.

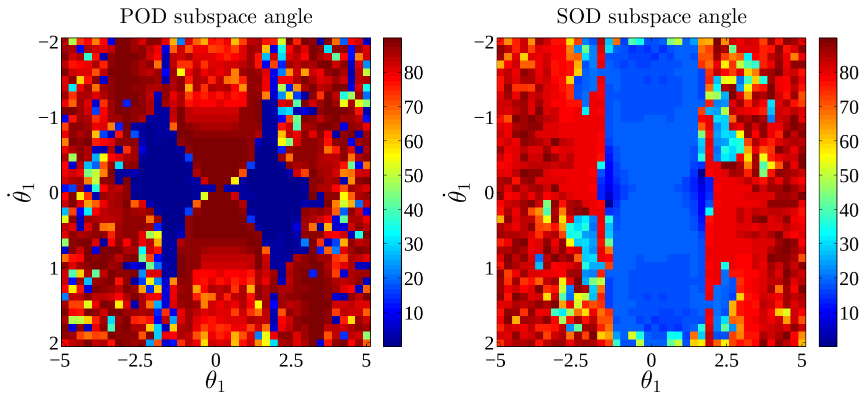

Figure 4: This figure shows how the angle of a 2D subspace changes with different energy level. The energy level is controlled by the initial condition. The figure is the phase plot of θ_1. With zero initial conditions for other state variables and the ones given on this plane, the system starts to vibrate and the angle of the corresponding 2D subspaces are calculated with respect to a reference 2D subspace.

2.3.1 A New Metric for Subspace Robustness

We observe that we obtain different modal subspaces for different energy levels of the systems which are imposed by changing initial conditions or external forcing. One of the goals of MOR in our work is to obtain a global subspace which is suitable for a range of variations in the energy level of a system under investigation. The conventional method for proper subspace identification for MOR is based on selecting those subspaces which capture most of the system's energy. However, this method would not assure that the subspace is suitable for ROM for an energy-varied system. Therefore, a new metric is required to measure if the obtained subspace is robust or not to the variations in systems' energy. In this section, we discuss a metric to measure the robustness of different subspaces with respect to each other.

We can change the systems subspaces obtained from multivariate analysis by changing systems' energy level in two ways: (1) changing the initial conditions of an unforced or forced system; and (2) changing the external forcing of a forced system. For example, we can vary the external forcing by changing its frequency content and/or forcing amplitude.

Regardless of how we change the systems' energy, we do s simulations or experiments and assemble the corresponding data matrices. We apply the intended multivariate analysis to the data and obtain s different modal spaces, $\mathcal{P}^1,\ \mathcal{P}^2,\ \ldots,\ \mathcal{P}^s$ corresponding to each simulation. The k-dimensional subspaces $\mathcal{P}_k^i$ and $\mathcal{P}_k^j$ of the modal space are considered linearly dependent if the minimal angle between them, denoted by θ_{ij}, is equal to zero. On the other hand they are said to be linearly independent, if $\theta_{ij} = \frac{\pi}{2}$.

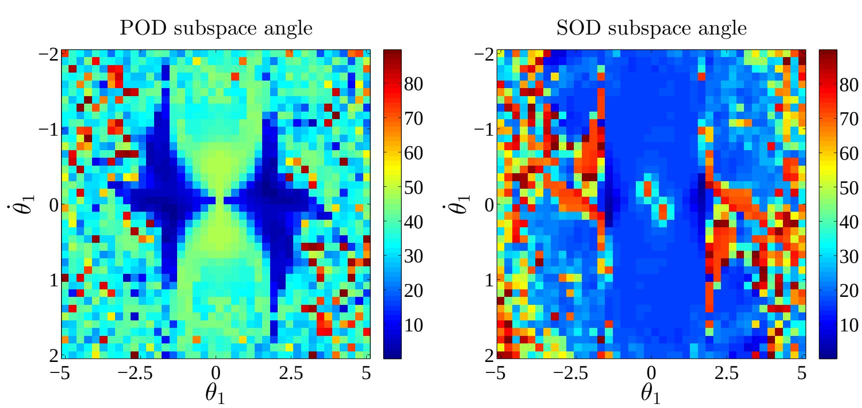

Figure 5: Subspace map in three dimensions

Each subspace $\mathcal{P}_k$ consists of k dominant modes. While these k individual modes can be totally different between two data sets, the subspace spanned by them can still be linearly dependent. For example, we need two LNMs to span a plane containing a damped linear oscillator degree-of-freedom in the n-dimensional vector space of a system. However, these modes are not unique—their linear combination would also span the same plane, which means that as the modes of system change with its energy level, they can still span the same subspace. Here, we propose a subspace robustness metric which determines if the MOR subspace is robust for a range of energy levels. The metric is a quantification of changes in the subspaces for the range of energies. For the subspace robustness close to one we can argue that the subspace is robust to the changes in energy level.

In case of s simulations it is difficult to simply use the angles between all the subspaces to develop a metric for subspace robustness. Here we propose to use singular values of all combined subspaces. Let us assume that k columns of matrix $\mathbf{P}_k^i$ span the k-dimensional subspace $\mathcal{P}_k^i$. We look at the vectors spanning the subspaces as data which live in the n-dimensional space and apply the singular value decomposition to find the principal directions within the data. We form the subspace robustness data matrix $\mathbf{S}$ by arranging the subspaces in the following order:

$$\mathbf{S} = \begin{bmatrix} \underbrace{\begin{bmatrix} \mathbf{p}_1^1, & \dots, & \mathbf{p}_k^1 \end{bmatrix}}_{\mathcal{P}_k^1 \text{ from } 1^{\text{st}} \text{ simulation}}, \underbrace{\begin{bmatrix} \mathbf{p}_1^2, & \dots, & \mathbf{p}_k^2 \end{bmatrix}}_{\mathcal{P}_k^2 \text{ from } 2^{\text{nd}} \text{ simulation}}, \dots, \underbrace{\begin{bmatrix} \mathbf{p}_1^s, & \dots, & \mathbf{p}_k^s \end{bmatrix}}_{\mathcal{P}_k^s \text{ from } \text{s}^{\text{th}} \text{ simulation}} \end{bmatrix}_{ks\times n}^T \tag{10}$$

From singular value decomposition of matrix $\mathbf{S}$, we obtain $2n$ direction vectors ϕ_i in the $2n$-dimensional space of data. The standard deviation of subspace data along vector ϕ_i is given by $\sigma_i = \|\boldsymbol{S}\phi_i\|$. We define $\boldsymbol{r}_k = \sum_{i=1}^{k} \sigma_i \phi_i$ to be the extension vector of the subspace data in the k-dimensional space. Then $\mathrm{Ker}(\boldsymbol{r}_k) = \sum_{i=k+1}^{2} n\sigma_i\phi_i$ is the extensiuon vector in the null space of the k-dimensional subspace. Thus, the total extension vector in the $2n$-dimensional space is $\boldsymbol{r}_n = \boldsymbol{r}_k + \mathrm{Ker}(\boldsymbol{r}_k)$. The magnitude of the kernel extension vector, $\|\mathrm{Ker}(\boldsymbol{r}_k)\|$, measures the leak of the data into the null space of the k-dimensional space. We compare this magnitude to that of the k-dimensional extension vector, $\|\boldsymbol{r}_k\|$. Therefore, the leak into higher dimensional space is evaluated by the angle of extension vectors in the k-dimensional space and its kernel as follows:

$$\alpha_k = \tan^{-1} \frac{\|\mathrm{Ker}(\boldsymbol{r}_k)\|}{\|\boldsymbol{r}_k\|} = \tan^{-1} \sqrt{\frac{\sum_{i=k+1}^{n} \sigma_i^2}{\sum_{i=1}^{k} \sigma_i^2}}. \tag{11}$$

We define a lower bound for α_k by taking the assumption that all the vectors spanning the subspaces are equally distributed in the space. In this case all singular values of matrix $\mathbf{S}$ are equal, i.e., $\sigma_i = \sigma$. Thus, a lower bound for the k-dimensional subspace, $\bar{\alpha}_k$, is:

$$\bar{\alpha}_k = \tan^{-1} \sqrt{\frac{\sum_{i=k+1}^{n} \sigma^2}{\sum_{i=1}^{k} \sigma^2}} = \tan^{-1} \sqrt{\frac{n-k}{k}}. \tag{12}$$

Using $\bar{\alpha}_k$ we map the angle $\bar{\alpha}_k \leq \alpha_k \leq \frac{\pi}{2}$ to 0 to 1 to define γ_k as follows:

$$\gamma_k = \frac{\bar{\alpha}_k - \alpha_k}{\bar{\alpha}_k}, \tag{13}$$

which we call the *subspace robustness* of the k-dimensional subspace.

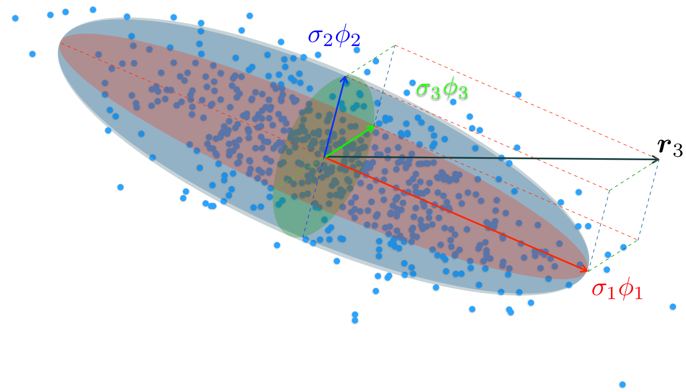

Figure 6: Geometric interpretation of subspace robustness

Geometric Interpretation: Fig. 6 depicts a schematic for a geometric interpretation of subspace robustness in a three-dimensional space. We assume that the modal space of the dynamical flow has three dimensions. $\mathbf{P}_i^s \in \mathbb{R}^3$ spans the modal space of the s-simulation data. We show the vectors spanning different subspaces as data points indicated by blue dots.

Singular value decomposition is applied to the whole data to obtain three components of the extension vectors shown in the figure. As an example, $\boldsymbol{r}_2 = \sigma_1\phi_1 + \sigma_2\phi_2$ is the two-dimensional covariance vector of data. $\mathrm{Ker}(\boldsymbol{r}_2) = \sigma_3\phi_3$ is the kernel covariance vector. We calculate the angle between the two-dimensional subspace and its kernel using Eq. (11):

$$\alpha_2 = \tan^{-1}\sqrt{\frac{\sigma_3^2}{\sigma_1^2+\sigma_2^2}} \tag{14}$$

A lower bound for two dimensional subspace of a three-dimensional space is defined via Eq. (12):

$$\bar{\alpha}_2 = \tan^{-1}\sqrt{\frac{1}{2}} \tag{15}$$

Now we can determine the robustness of our two-dimensional subspace via Eq. (13).

3 Reduced Order Nonlinear Control System

In order to construct ROM, we first randomly or stochastically drive the full-scale model to collect the required data from s different simulations. We use multivariate analysis to obtain the modal structure from each simulation. Then we apply the subspace robustness to the modal structures to select the dimension of the persistent subspace that can be used for the global reduced model. Using the obtained subspace we construct the model and compare it to the full-scale model.

While any record of the system states can be used as data for multivariate analysis, we use random excitation as the system input and collect the response of the system in the data matrices. This way we ensure that all neighbors of data points within the space of the system has been covered and that the modal structure we obtain from the analysis of data will be a better representation of the important dynamical characteristics of the system. Since we aim to build a *relatively global* reduced order control system which is valid for a range of energy levels, we do 12 simulations with different energy levels. To impose the changes in the energy, we only change the amplitude of the excitation while keeping the frequency content similar for all cases.

The link system has a linear modal frequency range up to $3\,\mathrm{Hz}$. We limit the frequency of the random excitation to $5\,\mathrm{Hz}$ to assure that all linear modes are covered while data are not contaminated by noise. We select 12 equally distributed choices of the random forcing amplitude from the range of $0.1 \leq q_0 \leq 3$. We excite the link system by the random forcing to obtain 12 data

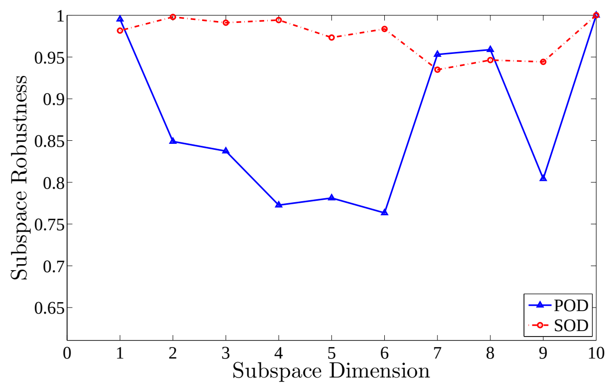

Figure 7: This figure shows the subspace robustness of both POD and SOD for different energy levels imposed by different random forcing. SOD subspace robustness is alway close to one while the POD one fluctuates.

matrices $\mathbf{Y}_1, \mathbf{Y}_2, \ldots, \mathbf{Y}_{12}$. We identify the modal structure of each data set using POD and SOD. We calculate the subspace robustness of POD and SOD modes using Eq. (13). Fig. 7 shows the subspace robustness of POD and SOD for each dimension. The POD subspace robustness for $k = 1$ is very close to unity which means that the first dominant POMs from all the simulations are linearly dependent. The POD subspace robustness is also close to one for $k = 7, 8$ and 10. On the other hand, the SOD subspace robustness is always close to one. A subspace robustness closer to one suggests few changes occur in subspaces from different simulation. This means that there is less leakage to the higher dimensional subspaces and the subspace is persistent to changes in system's energy level. Therefore, SOD subspaces, are more persistent compared to those of POD.

Following the identification of dimension for which the subspaces are robust and persistent, in order to obtain the global reduced order control model, we combine all the data matrices together to obtain a large response matrix, $\mathbf{Y}$, as follows:

$$\mathbf{Y} = \begin{bmatrix} \mathbf{Y}_1 \\ \vdots \\ \mathbf{Y}_{12} \end{bmatrix}. \tag{16}$$

We extract the corresponding POMs and SOMs, as the modal space given by $\mathbf{P}$, and its k-dimensional representation of the k dominant modes given by $\mathbf{P}_k$. In case k is the dimension of persistent subspace, we expect $\mathbf{P}_k$ via Eq. (2) to result in a persistent ROM within the range of energies of the nonlinear control system. Please note that for POD, POMs (denoted by ϕ) are orthogonal and thus, $\mathbf{P}_k = \phi_k$ and $\mathbf{P}_k^\dagger = \phi_k^T$. For SOD, however, SOMs and SPMs are bi-orthogonal ($\phi^T\psi = \mathbf{I}$), thus, $\mathbf{P}_k = \phi_k$ and $\mathbf{P}_k^\dagger = \psi_k^T$.

Also, from matrix $\mathbf{Y}$ we can extract POVs and SOVs to measure the dominance of the modes. Fig. 8 depicts the POVs and SOVs. We look for the drops in their values in order to identify the low-dimensional control models. There is no significant drop in the POVs for lower k values as we observe that they gradually decrease. The POV after $k = 8$ drops more drastically. However, SOVs come in pairs and the drops are distinguishable. A clear drops occur at $k = 2$, $k = 4$, and $k = 6$. Yet, we don't expect a good control model for $k = 2$ from SOD since the higher dimensional modes still have a significant SOV.

The full scale nonlinear control system will be controlled by a sequence of unit inputs. The proper choice of input merely depends on the design on the controller and the control method. Therefore, a *good* ROM for nonlinear control system is expected to mimic the output of the full scale model excited by a random input since we have no further knowledge about the specific controller.

We generate a filtered random input with the frequency content up to $5\,\mathrm{Hz}$. We excite both full-scale and ROM control systems by this input and compare their outputs, which are in this case the horizontal positions of the 5th link. For SOD, all the ROMs except for the three- and five-

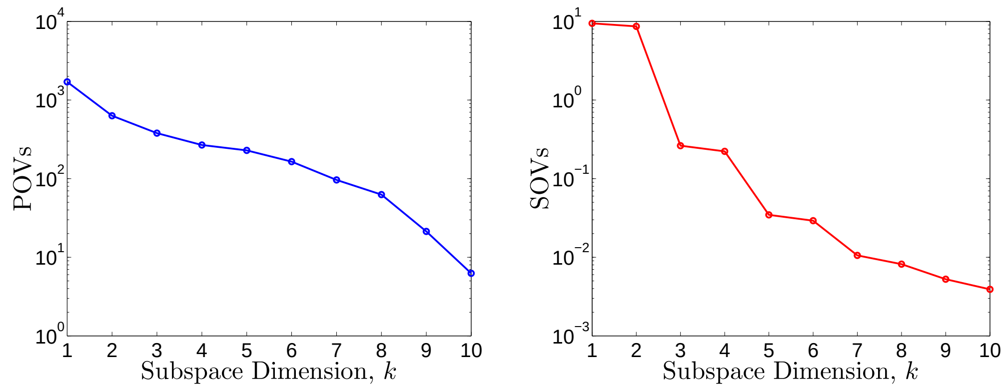

Figure 8: POVs compared to SOVs.

dimensional ones are stable, although the lowest dimensional ROM which provides good results is four-dimensional. In Fig. 9, we compare the output of the full-scale and the 4-dimensional SOD based ROM control system. These figures illustrate three different realization of random inputs. As we can see in the figures, the SOD control model closely follows the output of the control system. These results are consistent with the subspace robustness, which is always close to 1 for SOD, and the changes in SOVs in terms of the drop at $k = 4$.

POD ROMs are not stable for $k = 4,\ 5,\ 6$ and 7. The lower dimensional POD models are stable, though not able to closely follow the output. The 8-dimensional POD model may result in acceptable tracking as we can see in Fig. 10. In this figure we compare the output of the eight-dimensional POD model with that of the full-scale control system for the same random inputs that we used for the SOD models. Unlike four-dimensional SOD model, the eight-dimensional POD model outputs precedes the full control model outputs and their amplitudes are bigger. This confirms the results of the subspace robustness metric for POD.

In Fig. 11 we show the computation speed of the reduced control models and compare it to the full scale model of the control system. For both POD and SOD, the computation speeds of the unstable models are estimated by interpolation. We observe that the eight-dimensional POD model computation time is close to the full scale control model, while its performance is not as good. Nine- and ten-dimensional models are even slower than the full-scale model. We note that the ten-dimensional POD model is just a POD realization of the full-scale model with the same dimension. On the other hand, the four-dimensional SOD control model is more than 6 times faster than the full-scale model of the control system.

We also notice that the computation time of the SOD models, unlike POD, increases almost linearly. More interestingly, even a 10-dimensional SOD model, which has the same dimension as the full-scale model, is about twice faster, while it provides a perfect tracking of the output. We did

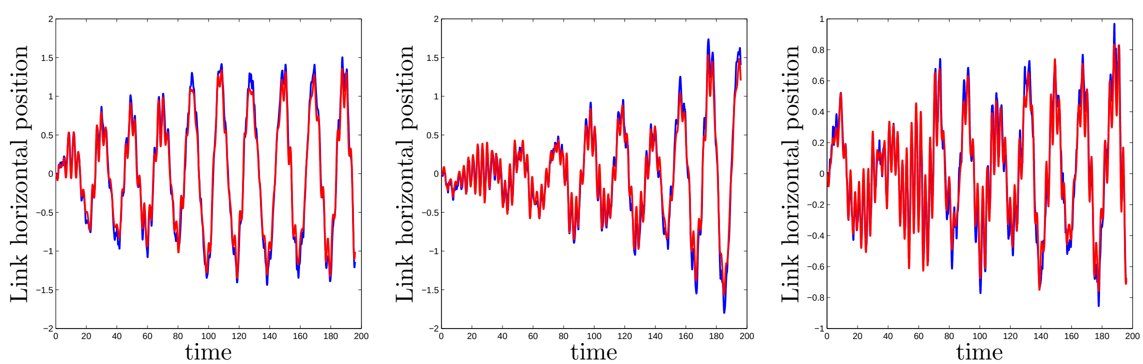

Figure 9: ROM on output of the control system using SOD for $k = 4$

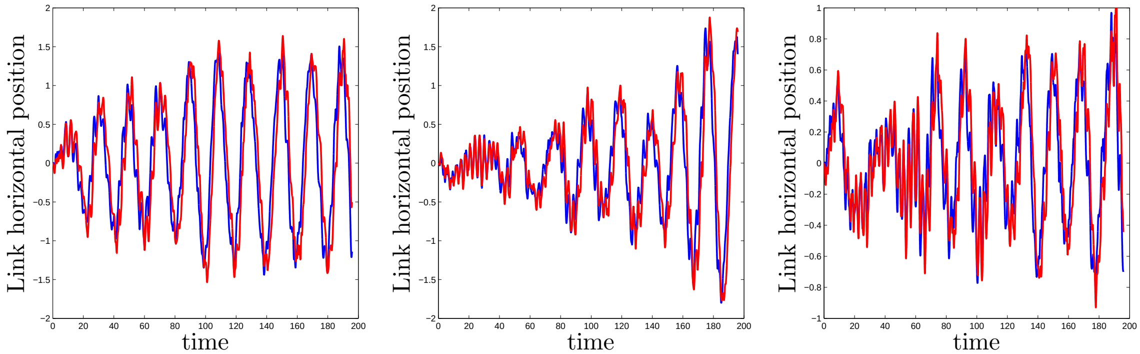

Figure 10: ROM on output of the control system using POD for $k = 8$.

not expect to get these results, however, at this point we speculate that SOD provides a smoother realization of the full-scale model of the control system. We will further investigate this effect in our future work.

4 Conclusions

A new approaches for MOR of nonlinear control systems was presented. An example of a system with five inverted links was used to examine our approach. The modal subspaces which were identified using projection based reduced order modeling methods were shown to dependent on the system's energy. The subspace robustness metric was proposed to obtain robust and persistent reduced order control models. These models were aimed to be valid for a range of the system's energy. The developed metric was used to evaluate for POD- and SOD-based subspaces. POD subspaces were shown persistent only for the high dimensional models. SOD subspaces were persistent for all the dimensions. The resultant reduced order control models were tested using different random inputs.

Low-dimensional POD-based ROMs were not stable and the high dimensional ones were not as accurate as the low-dimensional SOD ROMs. A four-dimensional SOD ROM closely tracked the output of the nonlinear control system to different random inputs. These results were consistent with the subspace robustness metric. The accurate SOD ROMs were shown to be six times faster than the full-scale model. These ROMs outperformed the best POD ROM, which was not significantly faster than the full-scale control system. Also, we showed that the smoothing effect of SOD may speed up the full-scale model simulations, as we observed that the 10-dimensional full-scale SOD model was as accurate as, but two times faster than the original full-scale system.

References

[1] Lall, S., Marsden, J. E., and Glavaški, S., 2002. "A subspace approach to balanced truncation for model reduction of nonlinear control systems". International journal of robust and nonlinear control, **12** (6) [], pp. 519–535.

[2] Ardeh, H. A., and Allen, M. S., 2013. "Investigating cases of jump phenomenon in a nonlinear oscillatory system". In *Topics in Nonlinear Dynamics, Volume 1*. Springer, pp. 299–318.

[3] Kuether, R. J., Brake, M. R., and Allen, M. S., 2014. "Evaluating convergence of reduced order models using nonlinear normal modes". In *Model Validation and Uncertainty Quantification, Volume 3*. Springer, pp. 287–300.

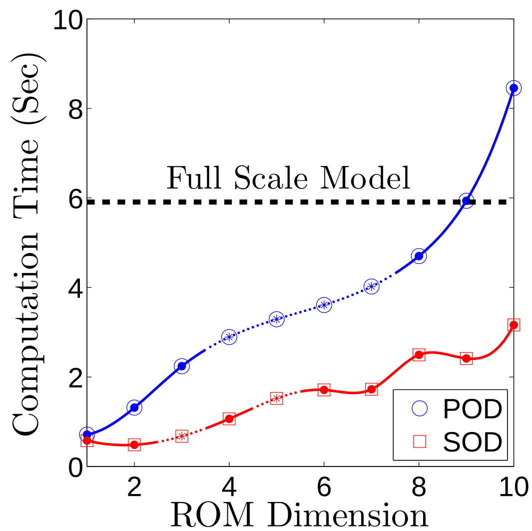

Figure 11: Computation time of POD and SOD based reduced order modeling

[4] Ilbeigi, S., and Chelidze, D. "Persistent model order reduction for complex dynamical systems using smooth orthogonal decomposition". *Mechanical Systems and Signal Processing (under review)*.

[5] Chelidze, D., and Zhou, W., 2006. "Smooth orthogonal decomposition-based vibration mode identification". Journal of Sound and Vibration, **292** (3) [], pp. 461–473.

[6] Ilbeigi, S., and Chelidze, D., 2016. "Reduced order models for systems with disparate spatial and temporal scales". In *Rotating Machinery, Hybrid Test Methods, Vibro-Acoustics & Laser Vibrometry, Volume 8*. Springer, pp. 447–455.

[7] Ilbeigi, S., and Chelidze, D., 2016. "Model order reduction of nonlinear euler-bernoulli beam". In *Nonlinear Dynamics, Volume 1*. Springer, pp. 377–385.

[8] Rathinam, M., and Petzold, L. R., 2003. "A new look at proper orthogonal decomposition". SIAM Journal on Numerical Analysis, **41** (5) [], pp. 1893–1925.

[9] Benner, P., Mehrmann, V., and Sorensen, D. C., 2005. *Dimension reduction of large-scale systems*, vol. 45. Springer.

[10] Antoulas, A. C., Ionutiu, R., Martins, N., ter Maten, E. J. W., Mohaghegh, K., Pulch, R., Rommes, J., Saadvandi, M., and Striebel, M., 2015. "Model order reductionmethods, concepts and properties".

[11] Maier, D., Hager, C., Hetzler, H., Fillot, N., Vergne, P., Dureisseix, D., and Seemann, W., 2015. "A nonlinear model order reduction approach to the elastohydrodynamic problem". *Tribology International,* **82** [], pp. 484–492.

[12] Kudryavtsev, M., Rudnyi, E., Korvink, J., Hohlfeld, D., and Bechtold, T., 2015. "Computationally efficient and stable order reduction methods for a large-scale model of mems piezoelectric energy harvester". Microelectronics Reliability, **55** (5) [], pp. 747–757.

[13] Benner, P., and Feng, L. "Model order reduction for coupled problems".

[14] Balajewicz, M., Amsallem, D., and Farhat, C., 2015. "Projection-based model reduction for contact problems". *arXiv preprint arXiv:1503.01000* [].

[15] Foias, C., Jolly, M., Kevrekidis, I., Sell, G., and Titi, E., 1988. "On the computation of inertial manifolds". Physics Letters A, **131** (7) [], pp. 433–436.

[16] Pesheck, E., Pierre, C., and Shaw, S., 2002. "A new galerkin-based approach for accurate non-linear normal modes through invariant manifolds". Journal of sound and vibration, **249** (5) [], pp. 971–993.

[17] Willcox, K., and Peraire, J., 2002. "Balanced model reduction via the proper orthogonal decomposition". AIAA journal, **40** (11) [], pp. 2323–2330.

[18] Benner, P., and Breiten, T., 2015. "Two-sided projection methods for nonlinear model order reduction". SIAM Journal on Scientific Computing, **37** (2) [], pp. B239–B260.

[19] Georgiou, I., 2005. "Advanced proper orthogonal decomposition tools: using reduced order models to identify normal modes of vibration and slow invariant manifolds in the dynamics of planar nonlinear rods". Nonlinear dynamics, **41** (1-3) [], pp. 69–110.

[20] Ghasemi, M., Yang, Y., Gildin, E., Efendiev, Y., Calo, V., et al., 2015. "Fast multiscale reservoir simulations using pod-deim model reduction". In SPE Reservoir Simulation Symposium, Society of Petroleum Engineers.

[21] Kerschen, G., Golinval, J.-c., Vakakis, A. F., and Bergman, L. A., 2005. "The method of proper orthogonal decomposition for dynamical characterization and order reduction of mechanical systems: an overview". Nonlinear dynamics, **41** (1-3) [], pp. 147–169.

[22] Stadlmayr, D., Witteveen, W., and Steiner, W., 2016. "Reduction of physical and constraint degrees-of-freedom of redundant formulated multibody systems". Journal of Computational and Nonlinear Dynamics, **11** (3) [], p. 031010.

[23] Stadlmayr, D., Witteveen, W., and Steiner, W., 2016. "A generalized constraint reduction method for reduced order mbs models". *Multibody System Dynamics* [], pp. 1–16.

[24] Stadlmayr, D., and Witteveen, W., 2016. "Model reduction for nonlinear multibody systems based on proper orthogonal-and smooth orthogonal decomposition". In *Nonlinear Dynamics, Volume 1*. Springer, pp. 449–457.

[25] Feldmann, P., and Freund, R. W., 1995. "Efficient linear circuit analysis by padé approximation via the lanczos process". Computer-Aided Design of Integrated Circuits and Systems, IEEE Transactions on, **14** (5) [], pp. 639–649.

[26] Glover, K., 1984. "All optimal hankel-norm approximations of linear multivariable systems and their l,-error bounds". International journal of control, **39** (6) [], pp. 1115–1193.

[27] Zhou, H., Su, X., Song, Y.-D., and Yan, Q., 2015. "Hankel-norm model reduction for delayed fuzzy systems". In Control and Decision Conference (CCDC), 2015 27th Chinese, IEEE, pp. 964–968.

[28] Rahrovani, S., Vakilzadeh, M. K., and Abrahamsson, T., 2014. "Modal dominancy analysis based on modal contribution to frequency response function 2-norm". Mechanical Systems and Signal Processing, **48** (1) [], pp. 218–231.

[29] Vakilzadeh, M. K., Rahrovani, S., and Abrahamsson, T., 2012. "An improved modal approach for model reduction based on input-output relation". In Int. Conf. on Noise and Vibration Engineering (ISMA)/Int. Conf. on Uncertainty in Struct. Dynamics (USD). Leuven, Belgium.

[30] Phillips, J. R., Daniel, L., and Silveira, L. M., 2003. "Guaranteed passive balancing transformations for model order reduction". Computer-Aided Design of Integrated Circuits and Systems, IEEE Transactions on, **22** (8) [], pp. 1027–1041.

[31] Baur, U., Benner, P., and Feng, L., 2014. "Model order reduction for linear and nonlinear systems: a system-theoretic perspective". Archives of Computational Methods in Engineering, **21** (4) [], pp. 331–358.

[32] Vakakis, A. F., 1997. "Non-linear normal modes (nnms) and their applications in vibration theory: an overview". Mechanical systems and signal processing, **11** (1) [], pp. 3–22.

[33] Kerschen, G., Peeters, M., Golinval, J.-C., and Vakakis, A. F., 2009. "Nonlinear normal modes, part i: A useful framework for the structural dynamicist". Mechanical Systems and Signal Processing, **23** (1) [], pp. 170–194.

[34] Lacarbonara, W., Rega, G., and Nayfeh, A., 2003. "Resonant non-linear normal modes. part i: analytical treatment for structural one-dimensional systems". International Journal of Non-Linear Mechanics, **38** (6) [], pp. 851–872.

[35] Nayfeh, A. H., 2011. *Introduction to perturbation techniques*. John Wiley & Sons.

[36] Kuether, R. J., and Allen, M. S., 2014. "A numerical approach to directly compute nonlinear normal modes of geometrically nonlinear finite element models". Mechanical Systems and Signal Processing, **46** (1) [], pp. 1–15.

[37] Nayfeh, A. H., and Mook, D. T., 2008. *Nonlinear oscillations*. John Wiley & Sons.

[38] Atwell, J. A., and King, B. B., 2001. "Proper orthogonal decomposition for reduced basis feedback controllers for parabolic equations". Mathematical and computer modelling, **33** (1) [], pp. 1–19.

[39] Bloch, A., and Marsden, J., 1989. "Controlling homoclinic orbits". Theoretical and Computational Fluid Dynamics, **1** (3) [], pp. 179–190.

[40] Ravindran, S. S., 2000. "A reduced-order approach for optimal control of fluids using proper orthogonal decomposition". International journal for numerical methods in fluids, **34** (5) [], pp. 425–448.

[41] Mustafa, D., and Glover, K., 1991. "Controller reduction by h-balanced truncation". IEEE Transactions on Automatic Control, **36** (6) [], pp. 668–682.

[42] Sun, M., and Lam, J., 2016. "Model reduction of discrete markovian jump systems with time-weighted h2 performance". International Journal of Robust and Nonlinear Control, **26** (3) [], pp. 401–425.

[43] Gugercin, S., and Antoulas, A. C., 2004. "A survey of model reduction by balanced truncation and some new results". International Journal of Control, **77** (8) [], pp. 748–766.

[44] Moore, B., 1981. "Principal component analysis in linear systems: Controllability, observability, and model reduction". IEEE transactions on automatic control, **26** (1) [], pp. 17–32.

[45] Garcia, C. E., Prett, D. M., and Morari, M., 1989. "Model predictive control: theory and practicea survey". Automatica, **25** (3) [], pp. 335–348.

[46] Antoulas, A. C., Sorensen, D. C., and Gugercin, S., 2001. "A survey of model reduction methods for large-scale systems". *Contemporary mathematics,* **280** [], pp. 193–220.

[47] Atwell, J. A., Borggaard, J. T., and King, B. B., 2001. "Reduced order controllers for burgers' equation with a nonlinear observer". Applied Mathematics And Computer Science, **11** (6) [], pp. 1311–1330.

[48] Rowley, C. W., 2005. "Model reduction for fluids, using balanced proper orthogonal decomposition". International Journal of Bifurcation and Chaos, **15** (03) [], pp. 997–1013.

[49] Smith, T. R., 2003. *Low-dimensional models of plane Couette flow using the proper orthogonal decomposition*.

[50] Scherpen, J. M., 1993. "Balancing for nonlinear systems". Systems & Control Letters, **21** (2) [], pp. 143–153.

[51] Scherpen, J. M., 1996. “H balancing for nonlinear systems”. International Journal of Robust and Nonlinear Control, **6** (7) [], pp. 645–668.

[52] Fujimoto, K., and Scherpen, J. M., 2010. “Balanced realization and model order reduction for nonlinear systems based on singular value analysis”. SIAM Journal on Control and Optimization, **48** (7) [], pp. 4591–4623.

[53] Van Der Veen, A.-J., Deprettere, E. F., and Swindlehurst, A. L., 1993. “Subspace-based signal analysis using singular value decomposition”. Proceedings of the IEEE, **81** (9) [], pp. 1277–1308.

Appendix A

$$\mathbf{M} = \begin{bmatrix} 1&0&0&0&0&0&0&0&0&0\\ 0&1&0&0&0&0&0&0&0&0\\ 0&0&1&0&0&0&0&0&0&0\\ 0&0&0&1&0&0&0&0&0&0\\ 0&0&0&0&1&0&0&0&0&0\\ 0&0&0&0&0&\frac{52}{3}&14\cos(y_1-y_2)&10\cos(y_1-y_3)&6\cos(y_1-y_4)&2\cos(y_1-y_5)\\ 0&0&0&0&0&14\cos(y_1-y_2)&\frac{40}{3}&10\cos(y_2-y_3)&6\cos(y_2-y_4)&2\cos(y_2-y_5)\\ 0&0&0&0&0&10\cos(y_1-y_3)&10\cos(y_2-y_3)&\frac{28}{3}&6\cos(y_3-y_4)&2\cos(y_3-y_5)\\ 0&0&0&0&0&6\cos(y_1-y_4)&6\cos(y_2-y_4)&6\cos(y_3-y_4)&\frac{16}{3}&2\cos(y_4-y_5)\\ 0&0&0&0&0&2\cos(y_1-y_5)&2\cos(y_2-y_5)&2\cos(y_3-y_5)&2\cos(y_4-y_5)&\frac{4}{3} \end{bmatrix} \tag{17}$$

$$\mathbf{L} = \begin{bmatrix} 0&0&0&0&0&1&0&0&0&0\\ 0&0&0&0&0&0&1&0&0&0\\ 0&0&0&0&0&0&0&1&0&0\\ 0&0&0&0&0&0&0&0&1&0\\ 0&0&0&0&0&0&0&0&0&1\\ \frac{-2k}{mL^2}&\frac{k}{mL^2}&0&0&0&\frac{-2b}{mL^2}&\frac{b}{mL^2}&0&0&0\\ \frac{k}{mL^2}&\frac{-2k}{mL^2}&\frac{k}{mL^2}&0&0&\frac{b}{mL^2}&\frac{-2b}{mL^2}&\frac{b}{mL^2}&0&0\\ 0&\frac{k}{mL^2}&\frac{-2k}{mL^2}&\frac{k}{mL^2}&0&0&\frac{b}{mL^2}&\frac{-2b}{mL^2}&\frac{b}{mL^2}&0\\ 0&0&\frac{k}{mL^2}&\frac{-2k}{mL^2}&\frac{k}{mL^2}&0&0&\frac{b}{mL^2}&\frac{-2b}{mL^2}&\frac{b}{mL^2}\\ 0&0&0&\frac{k}{mL^2}&\frac{-k}{mL^2}&0&0&0&\frac{b}{mL^2}&\frac{-b}{mL^2} \end{bmatrix} \tag{18}$$

$$\mathbf{f}_{\mathrm{n}} = \begin{bmatrix} 0\\ 0\\ 0\\ 0\\ 0\\ -14y_7^2\sin(y_1-y_2)-10y_8^2\sin(y_1-y_3)-6y_9^2\sin(y_1-y_4)-2y_{10}^2\sin(y_1-y_5)\\ 14y_6^2\sin(y_1-y_2)-10y_8^2\sin(y_2-y_3)-6y_9^2\sin(y_2-y_4)-2y_{10}^2\sin(y_2-y_5)\\ 10y_6^2\sin(y_1-y_3)+10y_7^2\sin(y_2-y_3)-6y_9^2\sin(y_3-y_4)-2y_{10}^2\sin(y_3-y_5)\\ 6y_6^2\sin(y_1-y_4)+6y_7^2\sin(y_2-y_4)+6y_8^2\sin(y_3-y_4)-2y_{10}^2\sin(y_4-y_5)\\ 2y_6^2\sin(y_1-y_5)+2y_7^2\sin(y_2-y_5)+2y_8^2\sin(y_3-y_5)+2y_9^2\sin(y_4-y_5) \end{bmatrix} \tag{19}$$